A Skeleton-Tree-Based Structural Retrieval Method for Spherical Hybrid Sliding Bearings

Fangting Liu[1], Yawen Fan[2,*], Jingfeng Shen[1,*], Zichuan Wang[1], Shikun Zhang[1]
[1]School of Mechanical Engineering, University of Shanghai for Science and Technology, Shanghai , China
[2]Sino-British International College, University of Shanghai for Science and Technology, Shanghai, China
[*]Corresponding Author

Abstract: To address the complex internal fluid-domain structure of Spherical Hybrid Sliding Bearings (SHSBs) and the inability of traditional geometric retrieval methods to capture topological features, this paper proposes an intelligent retrieval method based on skeleton trees. The bearing fluid-domain model is extracted by Boolean operations and uniformly voxelized. A topologically equivalent centerline skeleton is then extracted using the Euclidean distance transform and gradient vector flow (GVF) algorithm. Key feature nodes of the skeleton are identified using a 3 x 3 x 3 neighborhood convolution operator, and a four-dimensional global feature vector is constructed from the volume fraction, normalized skeleton length, number of endpoints, and number of branch points. Cosine similarity is finally used to achieve quantitative retrieval of bearing structures. Validation results show that the proposed method achieves a similarity of up to 99.9% for closely similar structures, effectively identifying geometric measure consistency and local topological differences.

Keywords: Spherical Hybrid Sliding Bearing; Structural Retrieval; Skeleton Tree; Fluid-Domain Topology; Gradient Vector Flow; Cosine Similarity

1. Introduction

Spherical Hybrid Sliding Bearings (SHSBs) are capable of withstanding both radial and axial loads and can effectively reduce friction and wear during lubrication. As a result, they offer comprehensive performance advantages including high rotational precision, high dynamic stiffness, excellent damping and vibration-reduction characteristics, and a long service life. These bearings have found widespread application in high-end equipment sectors such as ultra-precision machine tools and aerospace [1]. The performance of these bearings is highly dependent on the topological structure of their internal fluid domains, such as oil chamber layout, flow channel connectivity, and orifice configuration. Consequently, how to efficiently characterize and retrieve bearing structures to enable effective reuse of design knowledge has become a key issue in enhancing bearing design efficiency and innovation capabilities.

In the field of bearing design research, performance analysis and parameter optimization have always been key areas of focus. Ji et al. [2] employed the finite difference method to numerically solve the dynamic characteristics of SHSBs and analyzed the influence of structural parameters on bearing stiffness and damping coefficients. However, such studies often focus on the “analysis and optimization” of specific structures, lacking systematic mechanisms for “retrieving” and reusing existing design solutions.

Researchers have conducted extensive exploration in the field of 3D model structural characterization and shape retrieval. For point cloud skeleton extraction, Lu et al. [3] employed an improved adaptive k-means clustering algorithm to address the noise sensitivity of traditional methods; Fan et al. [4] integrated shape and skeleton features to propose a 3D point cloud object recognition method suitable for low-data-volume scenarios. Regarding the skeletonization of volumetric data, Menten et al. [5] proposed a differentiable skeletonization algorithm, integrating skeleton extraction into a gradient optimization framework. Heryan and Caliman [6] further evaluated the performance of methods such as

GVF in complex tubular structures and proposed an improved skeletonization algorithm. In the field of 3D shape retrieval, ROSA-Net proposed by Fu et al. [7] and the INRet framework proposed by Guan et al. [8] provide new technical pathways for high-precision 3D shape retrieval from the perspectives of structure-aware descriptors and implicit neural representation similarity metrics, respectively. Furthermore, the concepts of skeletons and central axes have demonstrated significant potential in the fields of engineering and computer vision. Azevêdo et al. [9] combined voxelization with surface capture techniques to achieve adaptive topological optimization in the fluid domain, providing a methodological reference for skeletonization of complex internal flow channels; Wang et al. [10] proposed an elastic shape analysis framework based on the extended square root of velocity function (SRVF), opening up new avenues for similarity measurement of tree-like skeletons.

In the field of mechanical engineering, Zhu Wenbo et al. [11] proposed a method for retrieving 3D models of mechanical parts based on skeleton trees. By extracting topological skeleton trees and constructing a similarity measurement model, they achieved efficient structural retrieval. Zhang et al. [12] further investigated algorithms based on skeleton similarity measurement, providing an effective approach for the automated matching of 3D models of mechanical parts. Wang et al. [13] proposed the JEANIE similarity metric method, which achieves precise matching of skeleton sequences through spatio-temporal and view-angle alignment of 3D skeleton sequences. These studies have laid a solid foundation for extending skeleton tree technology to structural retrieval of internal flow channels in SHSBs.

To address the shortcomings of existing bearing research—which focuses on performance simulation and parameter optimization but lacks a characterization of the internal flow channel topology—this paper proposes a bearing structure retrieval method based on a skeleton tree. By extracting the fluid domain and utilizing distance fields and gradient vector flow algorithms to construct a centerline skeleton, this method identifies key nodes through $3 \times 3 \times 3$ neighborhood convolution, constructs a four-dimensional feature vector, and employs cosine similarity to achieve quantitative structural retrieval.

2. Structural Characteristic Analysis of Spherical Hybrid Sliding Bearings

As core support components in high-end precision equipment, the core functions of SHSBs are realized through the complex flow field between their internal oil circulation system and the journal. This paper focuses on ultra-precision SHSBs used in marine propulsion systems, as shown in Figure 1.

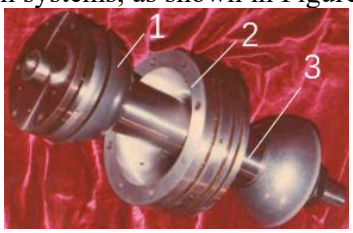

1. Front-convex ball 2. Rear-concave ball 3. Main shaft

(a) Ultra-precision SHSBs and their shafting

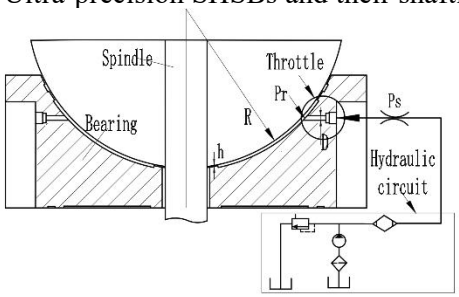

(b) Diagram of the working principle of a SHSB

Figure 1. Bearing Structure

The structural characteristics of this type of bearing can be defined as a closed, confined space formed by the bearing housing liner, the spherical journal, and the throttling system. From the perspective of structural retrieval, their performance similarity depends not only on the geometric dimensions of the external contour but, more fundamentally, on the topology and morphology of their internal oil passage system.

This study focuses on the following two aspects:

(1) It proposes the "lubrication channel topological framework" as the core characterization paradigm for the functional structure of fluid dynamic and hydrostatic bearings. This approach differs from traditional purely geometric descriptions or performance parameter descriptions, as it directly and concisely captures the key topological features that determine bearing performance.

(2) It introduces graph matching algorithms from computer science and adapts them to structural retrieval problems in the bearing field,

providing a concrete technical solution for achieving efficient, intelligent retrieval based on topological similarity.

3. Skeleton-Tree-Based Representation of Bearing Structures

To effectively characterize and retrieve complex internal flow channel structures in SHSBs, this study introduces a skeleton tree as an abstract model with a core topological structure. This method penetrates the geometric appearance of the solid model to directly capture its functional flow channel architecture, laying the foundation for subsequent similarity measurement and intelligent retrieval.

3.1 Definition of the Skeleton Tree

The skeleton, also known as the medial axis, was introduced by Blum [14] in 1967 and is defined as the set of centers of all maximal inscribed spheres within a 3D object. This definition endows the skeleton with two core geometric properties: centrality and topological equivalence. Two important properties of the skeleton are centrality and topological equivalence. Centrality ensures that the skeleton lies on the medial axis of the object, whereas topological equivalence indicates that the skeleton preserves the same topological structure as the original object, including the number of connected components and holes. A skeleton tree is obtained by discretizing the continuous skeleton and representing it as a graph. In this structure, branch nodes correspond to junctions between major components of the object, end nodes correspond to branch endpoints, and edges represent the connectivity between nodes. For subsequent analysis, the skeleton tree is defined as a graph structure obtained by abstracting the internal oil-circuit system in the three-dimensional solid model of SHSB, which is used to characterize the topological relationships and geometric features of the system.

This graph structure can be represented as $G = (V_s, E_s)$, where V_s denotes all skeleton vertices and E_s denotes the edges connecting adjacent skeleton vertices. The vertex set V_s represents functionally critical points, such as oil supply ports, return ports, and the centers of each oil chamber; the edge set E_s represents the centerlines of the flow channels connecting these vertices. This definition maps the geometric solid to a topological graph rich in functional information.

3.2 Bearing Structure Skeleton Extraction Algorithm

Given the complex, highly branched, and thin-walled nature of the oil-film space within SHSBs, this paper proposes a robust skeleton extraction framework (Figure 2).

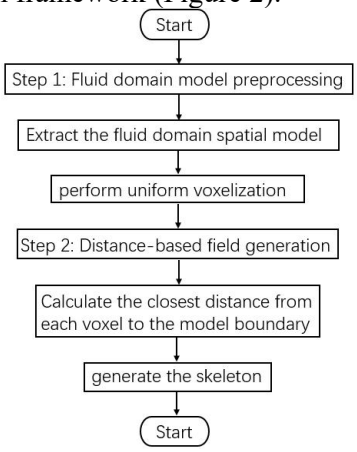

Figure 2. Framework of Bearing Skeleton Extraction

3.2.1 Fluid domain model preprocessing

The process begins with the input of the 3D model of SHSBs. Taking Model 1 in Figure 3 and Model 2 in Figure 4 as examples, their basic structural parameters are listed in Table 1. First, the fluid domain occupied by the lubricating oil is extracted by Boolean subtraction, as shown in Figures 3b and 4b. The extracted model is a solid composed of multiple interconnected closed cavities, which accurately represent the flow boundaries of the lubricating oil. The fluid-domain model is then uniformly voxelized, as shown in Figures 3c and 4c. Voxel resolution is a critical parameter: if it is too low, the skeletal structures of fine grooves, such as throttling grooves, may become disconnected; if it is too high, the computational cost increases substantially. Therefore, an adaptive strategy is adopted in this study to ensure that the narrowest flow-channel features are sampled with a width of at least three voxels.

3.2.2 Distance-field-based skeleton generation

Skeleton extraction is the foundation of structural retrieval. Its objective is to extract one-dimensional centerline structures from a discretized voxel model of a fluid domain that reflect its topological connectivity and geometric morphology. To achieve this goal, this paper first computes the Euclidean distance transformation field of the model, then identifies the centerline points based on the

features of the distance field, and finally obtains the initial skeleton using the gradient vector flow algorithm.

Table 1. Basic Bearing Specifications

Model	Model 1	Model 2
Bearing Inner Diameter R/mm	80	90
Number of Cavities	6	6
Cavity Depth d/mm	0.5	1
Capillary Tube Diameter D/mm	0.4	0.5
Bearing Clearance h/μm	30-50	30-50

(a) Model 1

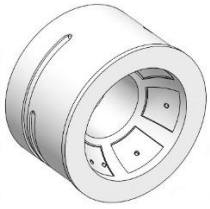

(a) Model 2

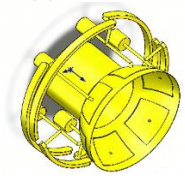

(b) Fluid domain spatial model of Model 1

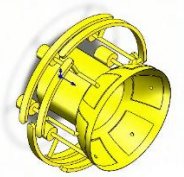

(b) Fluid domain spatial model of Model 2

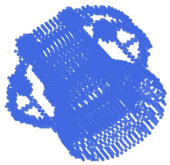

(c) Voxel model of Model 1

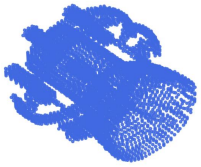

(c) Voxel model of Model 2

Figure 3. Model 1 and Its Fluid Domain Spatial Model.

Figure 4. Model 2 and Its Fluid Domain Spatial Model.

Let V denote a binary voxel grid, where $V(x,y,z)=1$ represents a voxel inside the fluid domain and $V(x,y,z)=0$ represents a voxel outside the fluid domain. First, the boundary voxel set ∂V of the fluid domain is extracted, consisting of those voxels that are inside the fluid domain and have at least one neighbor outside it, defined as:

$$\partial V=\{(x,y,z)|V(x,y,z)=1 \wedge \exists(x',y',z')\in N_6(x,y,z): V(x',y',z')=0\} \quad (1)$$

where $N_6(x,y,z)$ represents the 6-neighborhood (face-adjacent) of (x,y,z). This definition ensures that boundary voxels are located on the inner surface of the fluid domain, serving as the benchmark for distance field calculation.

The Euclidean distance transformation $D(x,y,z)$ is defined as the distance from the interior voxel (x,y,z) to the nearest boundary voxel:

$$D(x,y,z)=\min_{(i,j,k)\in\partial V}\sqrt[2]{(x-i)^2+(y-j)^2+(z-k)^2} \quad (2)$$

For any interior voxel $p=(x,y,z)$, calculate the distance from p to all boundary voxels q and take the minimum value, which is the shortest Euclidean distance:

$$D(p)=\min_{q\in\partial V}\| p-q \| \quad (3)$$

where ∂V denotes the set of boundary voxels and $\|\cdot\|$ represents the Euclidean norm. Geometrically, the distance $D(p)$ is equivalent to the radius of the maximum inscribed sphere centered at p and tangent to the boundary. The distance transform field $D(p)$ forms a scalar field within the entire fluid domain, with values increasing gradually from the boundary to the interior, providing a basis for subsequent medial axis identification.

According to midline transformation theory, for a three-dimensional region $\Omega\subset R^3$, its boundary is denoted by $\partial\Omega$. The midline $MA(\Omega)$ is defined as the set of all interior points that have at least two distinct nearest boundary points, that is:

$$MA(\Omega)=\{x\in\Omega|\text{ there exist at least two distinct boundary points } p,q\in\partial\Omega \text{ such that } d(x,p)=d(x,q)=d(x,\partial\Omega)\}$$

where $d(x,\partial\Omega)=\min_{y\in\partial\Omega}\| x-y \|$ denotes the minimum distance from point x to the boundary. This definition reveals the essential property of the medial axis as the "spine" of shape, consisting of the centers of all maximum inscribed spheres.

In a discrete voxel space, the above continuous definition must be transformed into a computable criterion. For a voxel $p=(x,y,z)$ to belong to the central axis, it must satisfy both of the following conditions:

(1) Distance from local maxima: Within the k-neighborhood $N_k(x,y,z)$ of , $D(p)$ is not less than the distance value of any neighboring voxel, i.e., $D(p)\geq D(q),\forall q\in N_k(p)\cap\Omega$. This ensures that p lies on the “ridge line” of the distance field.

(2) There exist at least two distinct boundary voxels $b_1, b_2\in\partial V$ such that $\| p-b_1 \|=\| p-b_2 \|=D(p)$, and b_1 and b_2 lie in different quadrants on the inscribed sphere of p. This

condition ensures that p indeed has at least two equidistant nearest boundary points.

where $N_k(p)$ denotes the K-neighborhood of p (typically $k = 26$), and b_1 and b_2 lie in different quadrants on the inscribed sphere of p. Directly enumerating all voxels and verifying the above conditions is computationally intensive and sensitive to noise; therefore, in practice, algorithms such as iterative refinement or gradient vector flow are typically used to gradually "erode" voxels from the boundary inward, ultimately yielding a skeleton line with a width of a single voxel.

The gradient vector flow method guides skeleton extraction by constructing a smooth vector field, effectively suppressing noise while preserving topological structure. First, define the gradient field ∇D of the distance field D:

$$\nabla D(p) = \left(\frac{\partial D}{\partial x}, \frac{\partial D}{\partial y}, \frac{\partial D}{\partial z}\right) \quad (4)$$

The partial derivatives are approximated using central differences:

$$\frac{\partial D}{\partial x} \approx \frac{[D(x+1,y,z) - D(x-1,y,z)]}{2\Delta x} \quad (5)$$

Similarly, we obtain $\partial D/\partial y$ and $\partial D/\partial z$.

The gradient vector field $v(x, y, z)$ is obtained as the diffusion field by solving the minimization of the functional:

$$E(v) = \iiint \mu \parallel \nabla v\parallel^2 + \parallel \nabla D\parallel^2 \parallel v - \nabla D\parallel^2 dxdydz \quad (6)$$

where μ is the regularization parameter, used to balance smoothness and data fidelity. The first term of this functional forces the vector field to vary gradually in smooth regions, while the second term encourages the vector field to approach the original gradient direction near the boundary. Minimizing this functional is equivalent to solving the corresponding Euler-Lagrange equation:

$$\mu\nabla^2 v - \left(v - \nabla D\right) \parallel \nabla D\parallel^2 = 0 \quad (7)$$

This equation can be solved using an iterative method:

$$v^{t+1} = v^{\mathrm{t}} + \Delta t\left[\mu\nabla^2 v^{\mathrm{t}} - \left(v^{\mathrm{t}} - \nabla D\right) \parallel \nabla D\parallel^2\right] \quad (8)$$

where ∇^2 denotes the Laplace operator and Δt is the iteration step size. Iterate until convergence to obtain a stable gradient vector flow field v.

In the converged vector field, the midline points satisfy the following characteristics:

$$\parallel v(p) \parallel \approx 0 \text{ and } \nabla^2 D(p) < 0 \quad (9)$$

That is, the norm of the gradient vector flow field approaches zero (indicating that the point lies on the "ridge line" of the distance field), and the Laplacian of the distance field is negative (reflecting that the point has local maximum curvature). By starting from the boundary voxels and progressively "eroding" inward toward voxels that do not satisfy the central axis condition, all voxels that meet the above conditions are ultimately retained, yielding the initial skeleton (as shown in Figure 5). This skeleton has a single-voxel width and fully preserves the topological connectivity of the original fluid domain.

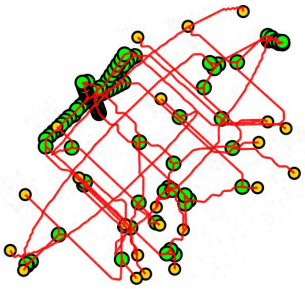

(a) Skeleton of Model 1

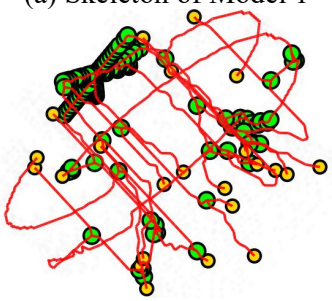

(b) Skeleton of Model 2

Figure 5. Initial Skeletons

4. Structural Similarity Retrieval Using Topological-Geometric Feature Vectors

To achieve automated retrieval of fluid domain structures in SHSBs, this paper proposes a similarity evaluation model that integrates spatial topological properties with geometric metrics. The model first performs topological analysis on the extracted digital skeleton using a $3 \times 3 \times 3$ spatial neighborhood convolution operator, identifying endpoints that characterize the tips of flow channels and branch points that characterize channel junctions by analyzing the statistical neighborhood response values. Subsequently, a four-dimensional global feature vector is constructed, comprising volume fraction, normalized skeleton length, the number of endpoints, and the number of branch points, to map the three-dimensional watershed model into a high-dimensional feature space. Finally, the cosine similarity algorithm is introduced to quantify the directional consistency between the feature vectors of the

two models, thereby deriving a similarity score for the bearing structures.

4.1 Spatial Neighborhood Convolution and Topological Feature-Point Extraction

Although the skeleton generated by the digital thinning algorithm depicts the central path of the flow channel, it still belongs to the low-level image data. To extract deep topological features, this paper defines a $3 \times 3 \times 3$ spatial neighborhood convolution operator K:

$$K(i,j,k) = 1,\ \ i,j,k \in \{-1,0,1\} \quad (10)$$

Let the distribution function of the digitized skeleton in three-dimensional discrete space be $S(x,y,z) \in \{0,1\}$. By performing spatial neighborhood convolution on the skeleton image, we obtain the topological response value $C(p)$ for each skeleton voxel:

$$C(x,y,z) = \sum_{i=-1}^{1}\sum_{j=-1}^{1}\sum_{k=-1}^{1} S(x+i,y+j,z+k) \quad (11)$$

According to the definition of connectivity in Euclidean space, the topological properties of a node p are determined by its neighborhood response value $C(p)$. Since the convolution calculation includes the central voxel itself, this paper defines the following classification criteria:

(1) End-points (E): If $C(p) = 2$, it indicates that the point is connected to only one neighboring point, representing a terminal point of a flow channel or a blind hole;

(2) Junction points (J): If $C(p) \geq 4$, this indicates that the point is connected to three or more points, representing a branch or convergence point of the flow channel.

Using the above operators, a complex geometric skeleton can be abstracted into a topological structure composed of sets of endpoints and junction points.

4.2 Construction of a Four-Dimensional Global Feature Vector

To eliminate the influence of the absolute dimensions of the bearing on the search results, this paper extracts geometric and topological information from the fluid domain and constructs a normalized four-dimensional global feature vector $F = [f_{vol}, f_{len}, f_{end}, f_{jun}]^T$ .The components are defined as follows:

(1) Volume fraction (f_{vol}): Describes the extent to which the fluid domain fills the bounding box:

$$f_{vol} = \frac{\sum V(x,y,z)}{R^3} \quad (12)$$

Here, $V(x,y,z)$ is the indicator function of the voxelized fluid domain, and R is the voxelization resolution.

(2) Normalized Skeleton Length (f_{len}):

$$f_{len} = \frac{\sum S(x,y,z)}{R} \quad (13)$$

This metric reflects the complexity and extent of the internal channels.

(3) End-node Density(f_{end}) and Junction-node Density (f_{jun}):

These are calculated directly from the total number of extracted key feature points, representing the structural closure and connectivity complexity, respectively.

4.3 Similarity Measurement Using Cosine Similarity

In the feature space, the structural similarity between two bearing models is transformed into a problem of directional consistency between their feature vectors F_1 and F_2 . This paper employs cosine similarity for quantification, which is calculated as follows:

$$Sim(F_1,F_2) = \cos\theta = \frac{\sum_{i=1}^{n} F_{1,i} \cdot F_{2,i}}{\sqrt{\sum_{i=1}^{n} F_{1,i}^2}\cdot\sqrt{\sum_{i=1}^{n} F_{2,i}^2}} \quad (14)$$

The similarity score $Sim \in [0,1]$. The advantage of this algorithm lies in its insensitivity to the absolute magnitude of feature components, enabling more effective identification of flow channel structures with similar topological proportions. When Sim approaches 1, it is determined that the two bearing fluid domains exhibit a high degree of consistency in terms of geometric compactness and topological connectivity.

5. Experimental Validation

To validate the effectiveness of the topology-geometry feature vector retrieval algorithm proposed in this paper, two sets of fluid-domain models of SHSBs (Model 1 and Model 2) were selected for comparative experiments. The two models exhibit a high degree of similarity in their macroscopic structures but exhibit minor differences in local details (such as the distribution of local grooves and flow channel branches).

At the same voxel resolution ($R = 64$), feature extraction was performed on both models using the algorithm proposed in this paper, yielding

the normalized four-dimensional global feature vector $F = [f_{vol}, f_{len}, f_{end}, f_{jun}]^T$, as shown in Table 2.

Table 2. Comparison of Feature Extraction Results for Fluid Domain Models

Feature item	Junction Point Count	Model 1	Model 2	Relative deviatio-n
Volume fraction	f_{vol}	5.0266×10^{-2}	5.0648×10^{-2}	0.76%
Normali-zed skeleton length	f_{len}	13.1250	13.0313	0.71%
Endpoint Count	f_{end}	27	23	14.81%
Junction Point Count	f_{jun}	96	99	3.13%

Analysis of the data in Table 2 reveals the following:

(1) Geometric consistency: As shown in Table 2, the volume fractions of Model 1 and Model 2 are 5.0266×10^{-2} and 5.0648×10^{-2}, respectively, and their normalized skeleton lengths are 13.1250 and 13.0313, respectively. The deviation between the two is less than 1%. This indicates that the overall flow channel scale and spatial footprint of the two models are highly consistent.

(2) Topological Differences: The number of endpoints (f_{end}) and the number of junctions (f_{jun}) reflect the local complexity of the structure. Model 1 has more endpoints (27) than Model 2 (23), indicating a richer network of terminal branches; meanwhile, Model 2 has a slightly higher number of junctions (99) than Model 1 (96), reflecting a slightly more complex internal connectivity structure.

Based on the extracted feature vectors $F_1 = [5.0266 \times 10^{-2}, 13.1250, 27, 96]^T$, $F_2 = [5.0648 \times 10^{-2}, 13.0313, 23, 99]^T$, the final matching scores for the two models were calculated using the cosine similarity algorithm:

$$Sim(F_1, F_2) = 0.9990$$

This result indicates that while the algorithm identifies a high degree of geometric similarity between the two models, it does not overreact to local structural variations (such as a difference of four endpoints). The sensitivity of the four-dimensional feature vectors to subtle structural changes in the fluid domain enables this method to distinguish between "closely related structures" with both robustness and precision.

6. Conclusions

This paper proposes a skeleton-tree-based intelligent retrieval method for the structural retrieval of spherical hybrid sliding bearings. The main conclusions are as follows:

(1) A topological representation method for bearing structures is established. By combining fluid-domain extraction and skeletonization, complex three-dimensional bearing structures are transformed into topologically equivalent skeleton-tree models, which effectively capture the connectivity of internal flow channels and provide a structured basis for similarity retrieval.

(2) A four-dimensional global feature vector composed of volume fraction, normalized skeleton length, endpoints, and branch points is constructed for structural characterization. The proposed feature representation is sensitive to subtle variations in the fluid domain. Simulation results show that the similarity can reach 99.9% for closely related structures, demonstrating the high discriminative capability of the method.

(3) This study has currently been validated only on two sets of closely related bearing models; future work is needed to further test the method's generality and robustness on larger-scale datasets. Additionally, while the four-dimensional feature vector currently employed is relatively concise, future work could incorporate graph neural networks to perform end-to-end learning on the skeleton tree, thereby achieving more precise similarity matching. Furthermore, integrating the retrieval results with CFD performance predictions to construct a "structure-performance" closed-loop optimization system represents a promising direction for future research.

References

[1] Li Y M. Ultra-high precision liquid hydrostatic spherical bearing system. Acta Metrologica Sinica, 1986(03):43-47.

[2] Ji D S, Shen J F, Chen Y F, et al. Dynamic characteristic analysis of spherical hybrid sliding bearings. Journal of Mechanical Strength, 2022, 44(2):1-8.

[3] Lu B, Fan X M. Research on 3D point cloud skeleton extraction based on improved adaptive k-means clustering. Acta Automatica Sinica, 2022, 48(8):1994-2006.

[4] Fan R J, Liu J, Yu J M, et al. Small sample 3D point cloud target recognition methodbased on shape and skeleton feature matching. Systems Engineering and Electronics, 2025, 48(1):76-86.

[5] Menten M J, Paetzold J C,Zimmer V A, et al. A skeletonization algorithm for gradient-based optimization//Proceedings of the IEEE/CVF International Conference on Computer Vision. 2023:21394-21403.

[6] Heryan K , Caliman T D . A Novel Skeletonization Algorithm for Topologically Complex Structures: Comparative Analysis and Application to Renal Arterial Trees. IEEE Access, 2025, 13(13):134989-135006.

[7] Rao Fu, Yunchi Zhang, Jie Yang, et al. ROSA-Net: Rotation-Robust Structure-Aware Network forFine-Grained 3D Shape Retrieval. Lecture Notes in Computer Science, 2024:295-319.

[8] Guan Y, Kwan D, Liang R, et al. INRet: A General Framework for Accurate Retrieval of INRs for Shapes//2025 International Conference on 3D Vision (3DV). IEEE, 2025:905-914.

[9] Anderson Soares da Costa Azevêdo, Li H, Ishida N ,et al. Body-fitted topology optimization via integer linear programming using surface capturing techniques. International journal for Numerical Methods in Engineering, 2024, 125(13):25.

[10] Wang G, Laga H, Srivastava A. Elastic shape analysis of tree-like 3d objects using extended srvf representation. IEEE transactions on pattern analysis and machine intelligence, 2023, 46(4):2475-2488.

[11] Zhu W B, Geng G Q, Liu Y Y, et al. 3D Model Retrieval Method of Mechanical Parts Based on Skeleton Tree. Journal of Mechanical Engineering, 2016, 52(13):204-212.

[12] Zhang X, Liu Y Y, Yang D. Three-dimensional Model Based on Mechanical Parts Skeleton Similarity Measure Algorithm. Nonferrous Metals Materials and Engineering, 2017, 38(4):234-238.

[13] Wang L, Liu J, Zheng L, et al. Meet JEANIE: A Similarity Measure for 3D Skeleton Sequences via Temporal-Viewpoint Alignment. International Journal of Computer Vision, 2024, 132(9):4091-4122.

[14] Ye F L. An Improved Image Skeleton Extraction Algorithm. Journal of Xichang University (Natural Science Edition), 2018, 32(3):91-93+123.

